Correction of Phase Errors in a Spin-Wave Transmission Line by Nonadiabatic Parametric Pumping

Roman Verba,[1,*] Mario Carpentieri,[2] Yu-Jin Chen,[3] Ilya N. Krivorotov,[3] Giovanni Finocchio,[4] Vasil Tiberkevich,[5] and Andrei Slavin[5]

[1]*Institute of Magnetism, Kyiv 03142, Ukraine*

[2]*Department of Electrical and Information Engineering, Politecnico di Bari, I-70125 Bari, Italy*

[3]*Department of Physics and Astronomy, University of California, Irvine, California 92697, USA*

[4]*Department of Electronic Engineering, Industrial Chemistry and Engineering, University of Messina, I-98166 Messina, Italy*

[5]*Department of Physics, Oakland University, Rochester, Michigan 48309, USA*

It is shown that phase errors in a microwave spin-wave transmission line can be corrected by subjecting the signal-carrying propagating spin wave to the action of a localized nonadiabatic parametric pumping, having the localization length smaller than the spin-wave wavelength. In such a transmission line the phase-transmission characteristic has a "steplike" shape containing flat "stabilization plateaus" separated by intervals of size π. Within the "plateau" regions the phase of the output spin wave is practically constant in a rather wide range of phases of the input spin wave. This effect can be used in magnonic logic devices for the correction of phase errors of up to $\pm 0.25\pi$. It is also proved that this phase-stabilization effect is stable against the variations of the spin-wave amplitude and is present across the amplitude range of the stable spin-wave propagation.

I. INTRODUCTION

Spin waves (SWs) propagating in nanoscale ferromagnetic waveguides are considered to be promising candidates for applications in a new generation of digital- and analog-signal-processing devices [1–5]. Recently, several novel concepts of magnonic logic elements and circuits have been proposed [6–12]. In magnonic logic, a digital signal can be coded via SW amplitude [6,13–15] or SW phase [2,16]. Obviously, in the case of phase-coded magnonic logic devices the spin-wave phase should be well defined, and should not fluctuate substantially in the course of the spin-wave propagation. This property of the SW phase stability is also crucial for amplitude-coded magnonic logic devices. Indeed, these devices often use SW interference for information processing and the phase relations between several processed SWs should be well defined for correct device operation [13,15,17,18].

For example, the result of the interference of two SWs having phases φ_1 and φ_2 and similar amplitudes is proportional to $\cos[(\varphi_1 - \varphi_2)/2]$. Deviation of the phase difference by 0.55π could be enough for incorrect interpretation of the interference result—instead of 1 in the ideal case $\varphi_1 - \varphi_2 = 0$ (or 0 if $\varphi_1 - \varphi_2 = \pi$), the resulting signal becomes less than 2/3 (greater than 1/3), which is commonly interpreted as indeterminate in amplitude-coded logic [15]. Deviation of the phase difference by 0.8π leads to a wrong result—logic "0" instead of "1" and vice versa.

There are several reasons for the SW phase deviation in a magnonic circle. The first is the deviation of the SW waveguide length due to lithographic misprints. This deviation can occur, for example, due to a misposition of the waveguide bends and a spread of bend shapes in a circuit. Small length deviations, not exceeding 1 nm at each bend, can accumulate over a magnonic circle and, for exemplary SWs of 100-nm wavelength, could reach critical values (corresponding to 0.55π phase shift) after passing several tens of such bends. Similarly, a misprint of the waveguide width leads to a change of SW dispersion and, thus, SW wave number at a fixed frequency, which is another source of random phase accumulation. Finally, stability of the SW phase can be violated by thermal fluctuations and the phase deviations leading, eventually, to a signal-processing error can accumulate in the course of the SW propagation in a magnonic circuit. Therefore, the timely correction of these phase errors is very important for stable and error-free operation of magnonic logic circuits.

In this work, we demonstrate that the problem of phase-error correction can be solved by application of localized parametric pumping, i.e., by using the interaction of a

___
*verrv@ukr.net

propagating SW with a localized microwave magnetic field (external or internal) of approximately double the SW frequency. Parametric pumping is a well-known method for excitation and amplification of SWs [19–22]. It is also known that parametric interaction becomes phase sensitive in the case of so-called "nonadiabatic" localized pumping, having a localization length (or other characteristic length of the spatial variation) that is smaller than the SW wavelength [23–25]. In our current work we calculate the phase-transmission characteristics for a SW transmission line containing a region where nonadiabatic parametric pumping is acting and show that the phase-transmission characteristics of such a line demonstrate "stabilization plateaus," within which the phase of the output SW signal is more or less constant in a rather wide range of phases of the input SW signal. Thus, the phase fluctuation of the SW signal acquired in the course of its propagation can be corrected. It is important that these phase-stabilization plateaus are separated by intervals of size almost exactly equal to π, which is thus perfectly suitable for phase-coded magnonic logic and/or signal processing.

II. THEORY

A sketch of the considered SW transmission line is shown in Fig. 1. It is a ferromagnetic nanowire of width w_y and thickness h. The SWs of the frequency ω_k, propagating in the $+x$ direction, are excited by the excitation gate or, in an integrated magnonic circuit, come from a preceding SW signal-processing device. The parametric pumping gate of length L_p is placed on the propagation path of the SWs. The parametric pumping can be created by a microwave magnetic field with polarization parallel to the direction of static magnetization of the nanowire [20,21], by the microwave electric field via various magnetoelectric effects [22], or by other means. The phase-stabilization effects discussed below do not depend on the nature of the pumping and are also independent of the direction of static magnetization of the nanowire.

To be specific with the coefficients used in our calculations, we consider the case of parametric pumping
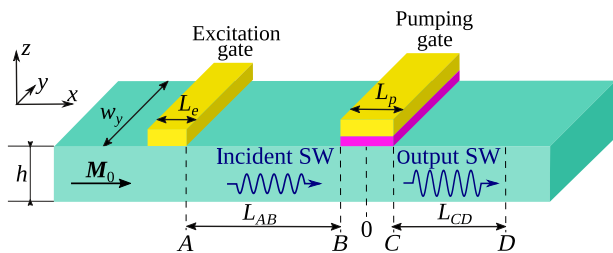

FIG. 1. A sketch of the considered magnonic transmission line showing regions of the SW excitation and the localization of the parametric pumping. The reference points *A–D* used in the in the micromagnetic simulations are also shown.

produced by a microwave voltage via the voltage-controlled magnetic anisotropy effect (VCMA) [26,27], which is the most efficient and convenient method for applications at the nanoscale. In this case the pumping gate consists of a strip of a normal metal separated by a dielectric layer from the conductive ferromagnetic material of the nanowire. The application of a microwave voltage of frequency ω_p to the gate results in oscillations of the perpendicular magnetic anisotropy at the ferromagnetic-dielectric interface with the same frequency [28,29]. It has been shown that these oscillations of anisotropy can couple parametrically to the SWs propagating in the nanowire, both in the case of the in-plane and out-of-plane static magnetization direction of the nanowire [22,29,30]. In the former case the coupling is stronger, and demonstrates no limits with respect to the SW wave number [30], so here we consider only this case of the in-plane static magnetization, as shown in Fig. 1.

In the parametric process of first order, the pumping is coupled to a pair of SWs having wave vectors k and k'. The efficiency of the parametric interaction is proportional to the $(k + k')$th Fourier harmonic $b_{p,k+k'}$ of the spatial distribution of the effective pumping field $b_p(x)$. Therefore, in the case of weakly localized quasiuniform pumping, when $kL_p \gg 1$, only the SWs with opposite wave vectors, $k' = -k$, interact efficiently with the pumping, which is a consequence of the momentum conservation law (the case of "adiabatic pumping").

In contrast, when the pumping localization length L becomes smaller than the SW wavelength (or if the pumping is spatially nonuniform with the characteristic length comparable to the SW wavelength), not only can the contrapropagating SWs ($k' = -k$) interact with the localized pumping field, but also other SWs ($k' \neq -k$), in particular copropagating SWs, can do so as well. This is the case of "nonadiabatic parametric pumping," as described in Ref. [23].

It should be noted that the parametric interaction has maximum efficiency when the resonance condition $\omega_p = \omega_k + \omega_{k'}$ is satisfied. This condition severely limits the number of SWs that can efficiently interact with the pumping. In the simple, and most common case, when the pumping frequency is twice as large as the SW frequency, $\omega_p = 2\omega_k$, the only SWs efficiently interacting with the nonadiabatic pumping are the above-mentioned contrapropagating SWs having the same modulus of SW wave vectors k and $-k$; however, the nonadiabatic term results in additional coupling of these SWs with themselves (that is the limiting case of the coupling of copropagating SWs, when approaching exact parametric resonance).

The SW dynamics under a localized parametric pumping is convenient to study using Bloembergen's system of equations. For the case of nonadiabatic pumping, it has been generalized in Ref. [23] and, neglecting the higher-order nonlinear SW interactions, it can be

written as

$$
\left(\frac{\partial}{\partial t} + v\frac{\partial}{\partial x} + \Gamma\right) a_1 = Vb_0 e^{-i\psi} a_2^* + Vb_{2k} e^{-i\psi} a_1^*,
$$
$$
\left(\frac{\partial}{\partial t} - v\frac{\partial}{\partial x} + \Gamma\right) a_2^* = Vb_0 e^{i\psi} a_1 + Vb_{2k} e^{i\psi} a_2. \tag{1}
$$

This system describes the evolution of the envelope amplitudes $a_1(x,t)$ and $a_2(x,t)$ of the two SW wave packets, having carrier wave vectors k and $-k$, respectively. In our problem, a_1 describes the envelope amplitude of the incident SW, which propagates toward the pumping region, and a_2 is the envelope amplitude of the idler SW, which is counterpropagating to a_1, and appears in the pumping region as a result of the parametric interaction. The relation of envelope amplitudes to the real magnetization amplitudes is given by the equation $\mathbf{m}_{1,2}(x,t) = [\mathbf{m}_k a_{1,2}(x,t) \exp(\pm ikx - i\omega_k t) + \text{c.c.}]$, where $\mathbf{m}_k$ describes the vector structure (ellipticity) of a particular SW. In Eq. (1), v and Γ are the group velocity and the damping rate of the SWs, V is the efficiency of the parametric coupling, ψ is the phase of the pumping, and $b_k = (1/L_p) \int_{-L_p/2}^{L_p/2} b_p(x) e^{ikx} dx$ is the Fourier harmonic of the effective field of pumping with the spatial profile $b_p(x)$. The fact that pumping is nonadiabatic is reflected by the last term in the equations, which describes the parametric coupling of the copropagating SWs ($k' = k$). In the case of quasiuniform adiabatic pumping this term is naturally absent, since $b_{2k} \to 0$. The value $\alpha = |b_{2k}/b_0|$ describes the strength of the nonadiabatic term relative to the adiabatic one, and is called "the degree of nonadiabaticity of the pumping."

In our particular case of the in-plane static magnetization and VCMA-induced pumping, the efficiency of the parametric coupling is given by $V = \gamma|m_{k,z}/4m_{k,y}|$, the pumping field is $b_p = 2\beta E/hM_s$ with β being the magnetoelectric coefficient, E is the amplitude of the microwave electric field applied to the pumping gate [30], and the pumping Fourier harmonics b_k are given by the expression $b_k = b_p \, \text{sinc}(kL_p/2) \equiv b_p \sin(kL_p/2)/(kL_p/2)$.

The pumping phase ψ is defined in such a way that the applied microwave electric field is $E(t) = E\sin(\omega_p t + \psi)$, with $\omega_p = 2\omega_k$ (exact parametric resonance). The real dynamic magnetization, corresponding to the steady propagating SW of the envelope amplitude $a_1 = |a_1|e^{-i\varphi}$, is $m_z(x,t) = 2m_{z,k}\sin(\omega_k t + \varphi - kx)$, where φ is the SW phase. Note that the point $x = 0$ is assumed to be at the center of the pumping gate, as shown in Fig. 1 and its position obviously affects the definitions of the phases φ and ψ. For other cases of the parametric pumping source and other directions of the static magnetization, the only differences in Eq. (1) come from the different values of the parametric coupling efficiency V [19,21,22], and the relations of the phases ψ and φ to the real time profiles

of the dynamic magnetization and applied pumping signal (microwave magnetic or electric field).

For further analysis it is convenient to introduce new real variables $A_{1\pm}$ and $A_{2,\pm}$, as $a_1 = e^{-i\psi/2}(A_{1+} + iA_{1-})$ and $a_2 = e^{-i\psi/2}(A_{2+} - iA_{2-})$, which is possible if the pumping is harmonic, i.e., if the pumping phase is time independent, $\psi \neq \psi(t)$. This operation, in fact, is a decomposition of a harmonic wave with an arbitrary phase into two partial waves, sine and cosine. Then, Eq. (1) is transformed to [23]

$$
\left(\frac{\partial}{\partial t} + v\frac{\partial}{\partial x} + \Gamma \mp Vb_{2k}\right) A_{1\pm} = Vb_0 A_{2\pm},
$$
$$
\left(\frac{\partial}{\partial t} - v\frac{\partial}{\partial x} + \Gamma \mp Vb_{2k}\right) A_{2\pm} = Vb_0 A_{1\pm}. \tag{2}
$$

As one can see, the pairs of partial waves (A_{1+}, A_{2+}) and (A_{1-}, A_{2-}) evolve independently and are connected only by the boundary conditions. The action of the nonadiabatic term Vb_{2k} results in different effective damping for partial waves: effective damping for the "in-phase" partial waves (A_{1+}, A_{2+}) is decreased, while the "out-of-phase" SWs (A_{1-}, A_{2-}) acquire an additional damping term. Thus, the partial waves evolve differently under the action of pumping, since the pumping pumps energy more effectively into the "in-phase" partial waves.

To find a steady-state solution of the transmission problem, we consider a stationary regime, setting $\partial A_i/\partial t = 0$. Equation (2) should be accompanied by a boundary condition $a_1(-L_p/2) = A_0 e^{-i\varphi_0}$, which describes the incoming SW with amplitude A_0 and arbitrary phase φ_0, and $a_2(L_p/2) = 0$, meaning that no idler wave is incident to the pumping region. Then, the envelope amplitude of the output SW $a_{out} = a_1(L_p/2)$ can be found to be

$$
a_{out} = A_0 e^{-i\psi/2}\left[\cos\left(\varphi_0 - \frac{\psi}{2}\right)K_+\right.
$$
$$
\left. - i\sin\left(\varphi_0 - \frac{\psi}{2}\right)K_-\right], \tag{3}
$$

where

$$
K_\pm = \left[\cos(\kappa_\pm L_p) + \frac{\tilde{\Gamma}_\pm}{v\kappa_\pm}\sin(\kappa_\pm L_p)\right]^{-1} \tag{4}
$$

are the amplification rates for partial waves, $\tilde{\Gamma}_\pm = \Gamma \mp Vb_{2k}$, and $\kappa_\pm^2 = (Vb_0)^2 - \tilde{\Gamma}_\pm^2$.

As usual [21], the parametric pumping results in a partial amplification of the incident SW, until the pumping amplitude reaches a certain threshold, at which a spontaneous generation of SWs takes place (the threshold of generation is determined from the condition $K_+ \to \infty$). Due to the nonadiabatic term, the amplification rates of the partial waves are different, resulting in the dependence of the

output SW amplitude on its phase [23,24]. Simultaneously, this means that the ratio between the amplitudes of the partial waves A_{1+} and A_{1-} changes within the pumping region, and is different at the end of the pumping gate compared to that at the gate entrance. Thus, the phase of the incident SW a_1 changes during the propagation through the pumping gate. Since the "in-phase" partial wave A_{1+} grows faster (or decays slower) than the "out-of-phase" partial wave, the phase of the incident wave approaches the phase of the "in-phase" partial wave, which is fixed by the phase of pumping to an accuracy of an integer multiple of π: $\varphi(x) \rightarrow \psi/2 + \pi n, n \in \mathbb{Z}$.

The phase-transmission characteristics are obtained from Eq. (3) simply as $\varphi_{out} = -Arg(a_{out})$. In the case of adiabatic pumping, when $b_{2k} = 0$, the phase-transmission characteristic is a simple straight line, $\varphi_{out} = \varphi_0$ [Fig. 2(a)]. Recall that the SW phase φ was introduced as a phase of the SW envelope, so the propagation phase shift kL_p is not taken into account in Fig. 2. This leads to a simple vertical shift of all the curves.

In contrast, as soon as the pumping becomes nonadiabatic, the SW phase-transmission characteristics become
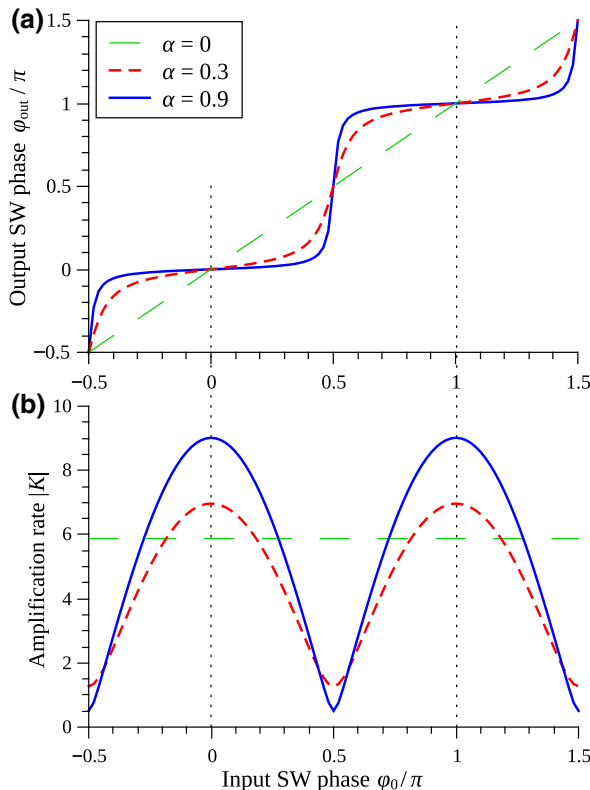

FIG. 2. (a) SW phase-transmission characteristics $\varphi_{out} = f(\varphi_0)$ and (b) amplification rates $|K| = f(\varphi_0)$ of a parametric pumping gate for different degrees of the pumping nonadiabaticity $\alpha = |b_{2k}/b_0|$. The pumping length $L_p = 0.1v/\Gamma$, the pumping strength is 90% of the SW generation threshold, and the pumping phase $\psi = 0$.

nonlinear. They demonstrate pronounced plateaus near the values $\varphi = 0, \pi$, which are the phases of the "in-phase" partial wave (since it is assumed that the pumping phase $\psi = 0$). Within these plateaus, the output SW phase is almost constant in a wide range of the input SW phases, i.e., nonadiabatic parametric pumping demonstrates the effect of SW phase stabilization. Importantly, the SW phase-stabilization plateaus are separated by phase intervals of size π, which perfectly matches the needs of the phase-coded magnonic logic, as under this approach the logic state "0" and the logic state "1" are coded by the SWs with a phase difference of π.

Stabilization plateaus become wider and more flat with an increase in the degree $\alpha = |b_{2k}/b_0|$ of the pumping "nonadiabaticity" [Fig. 2(a)]. A similar enhancement of the phase-stabilization properties is observed with an increase of the pumping strength, when this strength approaches the threshold of the parametric SW generation. In a limiting case, when $K_+ \gg K_-$ (which means that the pumping amplitude is close to the threshold or that the length of the pumping region is sufficiently large), the phase-transmission characteristic becomes almost a steplike function.

In should be noted that the pumping nonadiabaticity also results in the dependence of the output SW amplitude on the input SW phase, as shown in Fig. 2(b). When the phase stabilization becomes better, the variations of the SW amplitude also increase. Large variations of the SW amplitude, naturally, are not acceptable in SW processing devices, which limits the achievable ranges of the possible phase-error corrections in practice. Usually, about 10–15% of the SW amplitude variation can be considered acceptable, which defines the practical limits of the possible phase-error-correction interval as being about $\pm 0.25\pi$. Additional improvements can be achieved by placing a phase-insensitive amplitude-stabilization device after the phase stabilizer, which could use a nonlinear regime of the SW interaction with adiabatic pumping [31] or other nonlinear phenomena.

At the same time, a certain degree of SW amplitude variation can even be useful. When the SW phase is close to $\varphi_0 = \pi/2$, this means that the phase error is large and the interpretation of the SW phase as being the closest value to 0 or π may be incorrect. In the case of such large values of the phase errors it is often recommended to start the signal processing again. The above proposed phase-stabilization device indicates such large phase errors by a significant reduction of the amplitude of the output SW. In summary, by using the proposed phase-stabilization device small and moderate phase errors can be corrected, while the presence of large phase errors can clearly be determined and indicated.

Finally, we note that Fig. 2 illustrates the case when the phase stabilization is accompanied by amplification of the processed SWs. Often, this amplification is desirable

in magnonic circuits to compensate for propagation and processing losses, but sometimes a regime of no amplification [$K(0, \pi) \approx 1$] for in-phase waves needs to be realized. Fortunately, it is easy to vary the SW amplification rate by choice of the pumping amplitude and length. For example, the case of no amplification requires either a sufficiently long parametric pumping gate or enhanced magnetic damping within the parametric gate, so that the "out-of-phase" partial SWs decay significantly. The pumping nonadiabaticity in the case of a relatively long pumping gate can be realized by creating a spatially nonuniform pumping (e.g., a pumping gate consisting of several fingers having different polarities and/or strengths of the applied voltage). If the averaged pumping signal is nonzero (e.g., if fingers of opposite polarity are of unequal length), the SW dynamics is described by the same Eq. (1) in which the nonadiabatic term b_{2k} becomes large if $2k \approx 2\pi/P$, where P is the period of the fingers array. However, even in the case of zero averaged pumping one should expect the phase-stabilization effect to occur. In this case only the nonadiabatic term remains and one arrives at the limiting case of the parametric interaction of copropagating waves, when the idler wave is equivalent to the signal wave. In the case of copropagating waves, parametric pumping also can amplify waves (but cannot excite them) [32,33], and the nonadiabatic term is still phase sensitive; thus, one should expect qualitatively the same effect.

III. MICROMAGNETIC SIMULATIONS

To confirm our theoretical predictions about the SW phase stabilization we perform a series of micromagnetic simulations using the GPMagnet solver [34,35]. In our simulations the SWs are excited linearly by a microwave magnetic field applied at the excitation gate of length $L_e = 50$ nm. The excitation frequency is 6.49 GHz, which corresponds to a SW wavelength of 210 nm. Microwave parametric pumping in the form of modulation of the perpendicular anisotropy $\Delta K_\perp = b_p M_s \sin(\omega_p t)$ at a frequency $\omega_p/(2\pi) = 12.98$ GHz is applied at the pumping gate of length $L_p = 50$ nm, separated from the excitation gate by a distance $L_{AB} = 250$ nm. The corresponding degree of pumping nonadiabaticity in this case is $\alpha = 0.67$. To avoid the mistakes in the output SW phase determination due to the presence of the idler SW, the phase of the output SW is calculated at the point D. The SW phase at the end of the gate is retrieved by subtraction of the propagation phase accumulation kL_{CD}, where $L_{CD} = 250$ nm. The following material parameters of the Fe/MgO structure (common for VCMA experiments [36]) are used: saturation magnetization $\mu_0 M_s = 2.1$ T, exchange length $\lambda_{ex} = 3.4$ nm, surface perpendicular anisotropy energy $K_s = 1.36$ mJ/m^2, and effective Gilbert damping (including nonuniform broadening for a given SW frequency)

$\alpha_G = 0.02$. The nanowire thickness is set to $h = 1$ nm, the width is $w = 20$ nm, and the bias magnetic field is absent.

Simulations performed with no incident SW and a finite temperature of 1 K give a threshold of parametric excitation equal to $b_{p,\text{th}} = 130$ mT. It is somewhat smaller than the threshold of 169 mT calculated using the analytical equation Eq. (4) (from the condition $K_+ \to \infty$). We believe that the discrepancy is caused by the dispersion of SW group velocity.

In the simulations of the SW phase-transmission characteristics in the presence of an incident SW we set the pumping strength to $b_p = 100$ mT, which is 77% of the SW generation threshold. Thermal fluctuations are switched off to speed up the simulations—since we work sufficiently away from the threshold we do not expect a significant growth of thermal fluctuations under the parametric pumping gate. The simulated phase-transmission characteristic for small-amplitude (linear) SWs that are excited by a 1-mT excitation field are shown in Fig. 3 (blue dots). The figure shows definite phase-stabilization plateaus and matches well with the phase characteristics obtained in the analytical calculation (solid line) for a pumping strength equal to 77% of the theoretical SW generation threshold. We believe that the small upshift of the simulated phase characteristic is also related to the dispersion of the SW group velocity.

We also verify how phase-transmission characteristics change with the SW amplitude, when different nonlinear SW interactions become important. For this purpose we perform simulations for larger excitation fields, at 10 mT and 30 mT. For the excitation field of 30 mT the SW amplitude reaches a value of $M_y/M_s \approx 0.15$, which is definitely beyond the range where the excited SWs can be considered small amplitude (or linear) and in which our
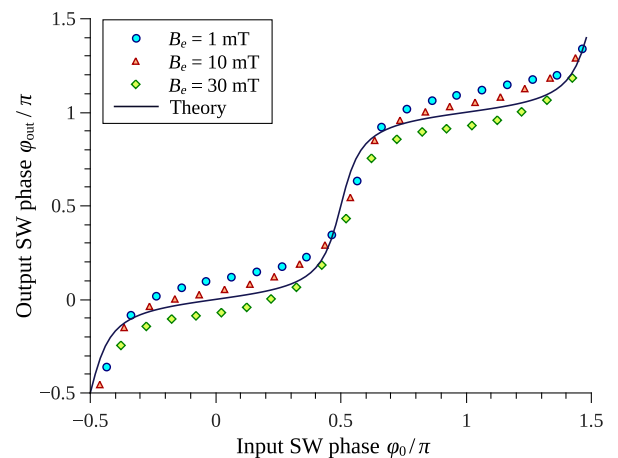

FIG. 3. Phase-transmission characteristics of a VCMA parametric pumping gate for different incident SW amplitudes created by different excitation fields B_e (symbols, micromagnetic simulations; solid line, theoretical curve for linear SWs).

analytical theory is valid. From Fig. 3 one can see that the phase-stabilization effect is still present in the case of the large-amplitude nonlinear SWs, and the sizes and slope of the phase-stabilization plateaus are almost the same, as in the linear case. The only difference is a downshift of these plateaus, which is a consequence of the nonlinear SW phase accumulation. Thus, nonadiabatic parametric pumping can be used for phase-error correction of both linear and nonlinear SWs.

IV. SUMMARY

In summary, we demonstrate that the interaction of a propagating SW with localized nonadiabatic parametric pumping leads to a shift of the SW phase, in addition to a simple propagation phase accumulation kL_p. As a result, the SW phase-transmission characteristics become nonlinear, demonstrating a "steplike" shape. They contain pronounced flat "stabilization plateaus," within which the output SW phase is almost constant in a certain range of phases of the input SW. The phase-stabilization effect becomes more pronounced with the increased level of the pumping nonadiabaticity and when the pumping strength approaches the threshold of the parametric SW generation (but it should not exceed the threshold). Our findings open a way for the implementation of phase-error corrections in magnonic logic circuits. The range of possible phase-error corrections is limited mainly by the phase dependence of the output SW amplitude and is about $\pm 0.25\pi$ for both linear and nonlinear SWs.

[1] V. V. Kruglyak, S. O. Demokritov, and D. Grundler, Magnonics, J. Phys. D: Appl. Phys. **43**, 264001 (2010).

[2] A. Khitun, M. Bao, and K. L. Wang, Magnonic logic circuits, J. Phys. D: Appl. Phys. **43**, 264005 (2010).

[3] S. O. Demokritov and A. N. Slavin, eds., *Magnonics. From Fundamentals to Applications* (Springer, Berlin, 2013).

[4] D. E. Nikonov and I. A. Young, Overview of beyond-CMOS devices and a uniform methodology for their benchmarking, Proc. IEEE **101**, 2498 (2013).

[5] M. Krawczyk and D. Grundler, Review and prospects of magnonic crystals and devices with reprogrammable band structure, J. Phys.: Cond. Matter. **26**, 123202 (2014).

[6] A. V. Chumak, A. A. Serga, and B. Hillebrands, Magnon transistor for all-magnon data processing, Nat. Commun. **5**, 4700 (2014).

[7] A. V. Chumak, V. I. Vasyuchka, A. A. Serga, and B. Hillebrands, Magnon spintronics, Nat. Phys. **11**, 453 (2015).

[8] S. Dutta, S.-C. Chang, N. Kani, D. E. Nikonov, S. Manipatruni, I. A. Young, and A. Naeemi, Non-volatile clocked spin wave interconnect for beyond-CMOS nanomagnet pipelines, Sci. Rep. **5**, 9861 (2015).

[9] A. Khitun, Parallel database search and prime factorization with magnonic holographic memory devices, J. Appl. Phys. **118**, 243905 (2015).

[10] K. Ganzhorn, S. Klingler, T. Wimmer, S. Geprägs, R. Gross, H. Huebl, and S. T. B. Goennenwein, Magnon-based logic in a multi-terminal YIG/Pt nanostructure, Appl. Phys. Lett. **109**, 022405 (2016).

[11] A. V. Sadovnikov, S. A. Odintsov, E. N. Beginin, S. E. Sheshukova, Yu. P. Sharaevskii, and S. A. Nikitov, Toward nonlinear magnonics: Intensity-dependent spin-wave switching in insulating side-coupled magnetic stripes, Phys. Rev. B **96**, 144428 (2017).

[12] Q. Wang, P. Pirro, R. Verba, A. Slavin, B. Hillebrands, and A. V. Chumak, Reconfigurable nanoscale spin-wave directional coupler, Sci. Adv. **4**, e1701517 (2018).

[13] T. Schneider, A. A. Serga, B. Leven, B. Hillebrands, R. L. Stamps, and M. P. Kostylev, Realization of spin-wave logic gates, Appl. Phys. Lett. **92**, 022505 (2008).

[14] B. Lenk, H. Ulrichs, F. Garbs, and M. Münzenberg, The building blocks of magnonics, Phys. Rep. **507**, 107 (2011).

[15] Q. Wang, R. Verba, T. Brächer, P. Pirro, and A. V. Chumak, "Integrated magnonic half-adder," arXiv:1902.02855 [physics.app-ph].

[16] S. Klingler, P. Pirro, T. Brächer, B. Leven, B. Hillebrands, and A. V. Chumak, Spin-wave logic devices based on isotropic forward volume magnetostatic waves, Appl. Phys. Lett. **106**, 212406 (2015).

[17] M. Balynsky, A. Kozhevnikov, Y. Khivintsev, T. Bhowmick, D. Gutierrez, H. Chiang, G. Dudko, Y. Filimonov, G. Liu, C. Jiang, A. A. Balandin, R. Lake, and A. Khitun, Magnonic interferometric switch for multi-valued logic circuits, J. Appl. Phys. **121**, 024504 (2017).

[18] B. Rana and Y. Otani, Voltage-Controlled Reconfigurable Spin-Wave Nanochannels and Logic Devices, Phys. Rev. Appl. **9**, 014033 (2018).

[19] V. S. L'vov, *Wave Turbulence under Parametric Excitation* (Springer-Verlag, New York, 1994).

[20] A. G. Gurevich, and G. A. Melkov, *Magnetization Oscillations and Waves* (CRC Press, New York, 1996), p. 464.

[21] T. Brächer, P. Pirro, and B. Hillebrands, Parallel pumping for magnon spintronics: Amplification and manipulation of magnon spin currents on the micron-scale, Phys. Rep. **699**, 1 (2017).

[22] R. Verba, M. Carpentieri, G. Finocchio, V. Tiberkevich, and A. Slavin, in *Spin Wave Confinement: Propagating Waves (2nd Edition)*, edited by S. O. Demokritov (Singapore, Pan Stanford Publishing Pte. Ltd., 2017), p. 385.

[23] G. A. Melkov, A. A. Serga, V. S. Tiberkevich, Yu. V. Kobljanskij, and A. N. Slavin, Nonadiabatic interaction of a propagating wave packet with localized parametric pumping, Phys. Rev. E **63**, 066607 (2001).

[24] A. A. Serga, S. O. Demokritov, B. Hillebrands, Seong-Gi Min, and A. N. Slavin, Phase control of nonadiabatic parametric amplification of spin wave packets, J. Appl. Phys. **93**, 8585 (2003).

[25] T. Brächer, F. Heussner, P. Pirro, T. Meyer, T. Fischer, M. Geilen, B. Heinz, B. Lägel, A. A. Serga, and B. Hillebrands, Phase-to-intensity conversion of magnonic spin currents and application to the design of a majority gate, Sci. Rep. **6**, 38235 (2016).

[26] M. Weisheit, S. Fähler, A. Marty, Y. Souche, C. Poinsignon, and D. Givord, Electric field-induced modification of magnetism in thin-film ferromagnets, Science **315**, 349 (2007).

[27] C.-G. Duan, J. P. Velev, R. F. Sabirianov, Z. Zhu, J. Chu, S. S. Jaswal, and E. Y. Tsymbal, Surface Magnetoelectric Effect in Ferromagnetic Metal Films, Phys. Rev. Lett. **101**, 137201 (2008).

[28] J. Zhu, J. A. Katine, G. E. Rowlands, Y.-J. Chen, Z. Duan, J. G. Alzate, P. Upadhyaya, J. Langer, P. K. Amiri, K. L. Wang, and I. N. Krivorotov, Voltage-Induced Ferromagnetic Resonance in Magnetic Tunnel Junctions, Phys. Rev. Lett. **108**, 197203 (2012).

[29] Y.-J. Chen, H. K. Lee, R. Verba, J. A. Katine, I. Barsukov, V. Tiberkevich, J. Q. Xiao, A. N. Slavin, and I. N. Krivorotov, Parametric resonance of magnetization excited by electric field, Nano Lett. **17**, 572 (2017).

[30] R. Verba, M. Carpentieri, G. Finocchio, V. Tiberkevich, and A. Slavin, Excitation of Spin Waves in an In-Plane-Magnetized Ferromagnetic Nanowire Using Voltage-Controlled Magnetic Anisotropy, Phys. Rev. Appl. **7**, 064023 (2017).

[31] R. Verba, M. Carpentieri, G. Finocchio, V. Tiberkevich, and A. Slavin, Amplification and stabilization of large-amplitude propagating spin waves by parametric pumping, Appl. Phys. Lett. **112**, 042402 (2018).

[32] N. Bloembergen, *Nonlinear Optics* (W.A. Benjamin Inc., New York, 1965).

[33] R. Verba, V. Tiberkevich, and A. Slavin, Influence of interfacial Dzyaloshinskii-Moriya interaction on the parametric amplification of spin waves, Appl. Phys. Lett. **107**, 112402 (2015).

[34] L. Lopez-Diaz, D. Aurelio, L. Torres, E. Martinez, M. A. Hernandez-Lopez, J. Gomez, O. Alejos, M. Carpentieri, G. Finocchio, and G. Consolo, Micromagnetic simulations using graphics processing units, J. Phys. D: Appl. Phys. **45**, 323001 (2012).

[35] V. Puliafito, A. Giordano, A. Laudani, F. Garescì, M. Carpentieri, B. Azzerboni, and G. Finocchio, Scalable synchronization of spin-hall oscillators in out-of-plane field, Appl. Phys. Lett. **109**, 202402 (2016).

[36] T. Maruyama, Y. Shiota, T. Nozaki, K. Ohta, N. Toda, M. Mizuguchi, A. A. Tulapurkar, T. Shinjo, M. Shiraishi, S. Mizukami, Y. Ando, and Y. Suzuki, Large voltage-induced magnetic anisotropy change in a few atomic layers of iron, Nature Nano. **4**, 158 (2009).